Chemosphere 287 (2022) 132370

Contents lists available at ScienceDirect

Chemosphere

journal homepage: www.elsevier.com/locate/chemosphere

High-performance carbon black electrode for oxygen reduction reaction and oxidation of atrazine by electro-Fenton process

Okan Karatas [a,b], Nevin Atalay Gengec [c], Erhan Gengec [d], Alireza Khataee [a,e,*], Mehmet Kobya [a,f]

[a] Department of Environmental Engineering, Gebze Technical University, 41400, Gebze, Turkey
[b] Department of Environmental Engineering, Bursa Technical University, 16310, Bursa, Turkey
[c] Department of Chemical Engineering, Bilecik Şeyh Edebali University, 11230, Bilecik, Turkey
[d] Department of Environmental Protection, University of Kocaeli, 41275, Izmit, Kocaeli, Turkey
[e] Research Laboratory of Advanced Water and Wastewater Treatment Processes, Department of Applied Chemistry, Faculty of Chemistry, University of Tabriz, 51666-16471, Tabriz, Iran
[f] Kyrgyz-Turkish Manas University, Department of Environmental Engineering, Bishkek, Kyrgyzstan

HIGHLIGHTS

- Hydrophobic electrodes are produced by simple press of carbon black.
- 409 mg/L hydrogen peroxide was obtained with the produced CB electrodes.
- The electrodes showed high stability in H_2O_2 production and electro-Fenton.
- 99% Atrazine degradation was achieved with electro-Fenton in short times.

GRAPHICAL ABSTRACT

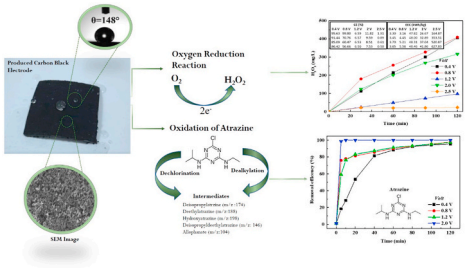

ARTICLE INFO

Handling Editor: Hassan Karimi-Maleh

Keywords:
Atrazine
Hydrogen peroxide
Electro-oxidation
Electro-fenton
Carbon black

ABSTRACT

The aim of this study is to produce an electrode that can be used in H_2O_2 production and Electro-Fenton (EF) process by an effective, cheap, and easy method. For this reason, a superhydrophobic electrode with a higher PTFE ratio and high thickness was produced with a simple press. The produced electrode was used in the production of H_2O_2 and mineralization of Atrazine. First, the effect of pH, cathode voltage, and operation time on H_2O_2 production was evaluated. The maximum H_2O_2 concentration (409 mg/L), the highest current efficiency (99.80%), and the lowest electrical energy consumption (3.16 kWh/kg) were obtained at 0.8 V, 7.0 of pH, and 120 min, and the stability of the electrode was evaluated up to 720 min. Then, the effects of the operational conditions (pH, cathode voltage, operating time, and catalyst concentration) in electro-Fenton were evaluated. The fastest degradation of Atrazine (>99%) was obtained at 2.0 V, 3.0 of pH, and 0.3 mM of Fe^{2+} in 15 min. In the final part of the study, the degradation intermediates were identified, and the characterization of the electrode was evaluated by SEM, XRD, FT-IR, tensiometer, potentiostat, and elemental analyzer.

* Corresponding author.
E-mail addresses: akhataee@gtu.edu.tr, a_khataee@tabrizu.ac.ir (A. Khataee).

https://doi.org/10.1016/j.chemosphere.2021.132370
Received 18 August 2021; Received in revised form 17 September 2021; Accepted 24 September 2021
Available online 27 September 2021

1. Introduction

Hydrogen peroxide (H_2O_2), an environmentally friendly oxidant over the whole pH range, is used in a great deal of the industrial area such as treatment of wastewater, synthesis of organic compounds, pulp and bleaching, disinfection, and waste gas treatment. Nowadays, water treatment is one of the significant reasons increase in industrial demand for H_2O_2. The centralized production of H_2O_2 has some disadvantages, such as transportation, storage, and handling problems. On the other hand, the on-site production method of H_2O_2 based on a two-electron of oxygen reduction reaction (ORR; Eqn. (1)) at the cathode eliminates these problems. However, this cathodic process needs to be developed to produce higher concentrations of H_2O_2. For this reason, studies to increase the yield in the H_2O_2 production process based on ORR are a very intensive research area in literature. Despite this disadvantage, various industrial processes only require H_2O_2 with a concentration lower than 9 wt% such as wastewater treatment (only <0.1 wt%), chemical synthesis, medical disinfection, pulp bleaching, and cosmetic uses (Zhou et al., 2019).

When H_2O_2 is used in the presence of a catalyst, usually in acidic conditions (nearly 3.0 of pH), a very powerful radical, $OH^{\bullet}$ (Eqn. (2), 2.80 V versus NHE), is formed, and this process is called Fenton (Ghasemi et al., 2020; Jiang et al., 2020; Mehdizadeh et al., 2020; Ribeiro and Nunes, 2021; Shen et al., 2021; Yao et al., 2021) If H_2O_2 is obtained with ORR at cathode, it is called Electro-Fenton (EF). The idea of producing H_2O_2 in situ in the EF process has additional advantages such as catalysis regeneration at the cathode (Eqn. (3)) (Ergan and Gengec, 2020; Khataee et al, 2009, 2014, 2017; Ribeiro and Nunes, 2021; Xuan et al., 2015)

$$0_2 + 2H^+ + 2e^- \rightarrow H_2O_2 (0.695\ \ V\ \ vs.SHE) \quad (1)$$

$$Fe^{2+} + H_2O_2 + H^+ \leftrightarrow Fe^{3+} + H_2O + OH^{\bullet}\ (2.8\ V\ vs.\ SHE) \quad (2)$$

$$Fe^{3+} + e^- \rightarrow Fe^{2+} (0.77\ \ V\ \ vs.SHE) \quad (3)$$

Since the cathode material plays a decisive role in H_2O_2 production, the effectiveness of many electrodes such as Boron Doped Diamond (BDD), metal-metal oxide (MMO), and carbon-based electrodes such as graphite, activated carbon fiber, carbon felt, reticulated vitreous carbon, carbon foam, carbon sponge, graphene, and carbon nanotubes composites have been investigated (Paz et al., 2018; Zhou et al., 2014). However, especially carbon-based ones come into prominence with their relatively high treatment efficiencies due to high over-potential for H_2 evolution, favoring H_2O_2 formation. Furthermore, carbon-based material is nontoxic and exhibits commercial availability with low costs. However, for the widespread use in the treatment of real wastewater, especially containing some resistant pollutants, deficiencies of carbon-based electrodes such as more active surface area and long-term stability need to be solved.

In this study, an electrode with roughnesses in the form of micro and nano/microfiber was produced with a simple, inexpensive, and fast method by a simple press. Firstly, the obtained superhydrophobic electrode with a higher PTFE ratio and high thickness was used in the production of H_2O_2 and the effect of process parameters (pH, Voltage, and operating time) was determined. The maximum in-situ H_2O_2 production was obtained as 409 mg/L which shows the importance of the study. Then, the electrode was used as a cathode in Electro-Fenton (EF) process, and the effect of pH, Voltage, operating time, and catalyst concentration on Atrazine removal was determined.

2. Experimental section

2.1. Materials

The Carbon Fiber (CF) was supplied from a commercial market in Turkey and Carbon Black (CB) was purchased from Nanografi. The electrolyte (anhydrous, $Na_2SO_4 \geq$ 99.0–100.5%), catalyst ($FeSO_4{\cdot}7H_2O$, 99%), and some other chemicals (potassium iodide (KI, $\geq$ 99.5%), ammonium molybdate tetrahydrate ($(NH_4)_6Mo_7O_{24}{\cdot}4H_2O \geq$ 99.0%), potassium hydrogen phthalate (KHP $\geq$99.5%), H_2SO_4, and NaOH (for adjustment of the solution pH) were supplied from Merck. The Atrazine and some of the other chemicals ($K_3[Fe(CN)_6]$, and KCl) were received from Sigma-Aldrich Chemistry. N_2 and O_2 gases (99.9%) were received from a local supplier.

2.2. The preparation of cathodes

The 5 g of CB were filled into a capped flask with 100 mL EtOH and 4 g of PTFE were added. It was sonicated in a sonic bath for 40 min and then shaking in an orbital shaker for 30 min to obtain a homogeneous mixture. The homogeneous mixture was carefully poured into the glass Petri dish, and the EtOH was evaporated at 80 °C up to get a paste. Then CF was placed in a press as supporting material, and the paste was put on the CF. The press was adjusted to 200 bar and 320 °C degrees. After the press cools down in ambient conditions, the impurities on the electrode were removed with acetone and distilled water. The prepared electrode was kept at 80 °C overnight.

2.3. Characterization of electrodes

A Scanning Electron Microscopy (SEM, Hitachi, Germany) was used for observing the surface morphologies of electrodes (Karimi-Maleh et al., 2022; Orooji et al., 2021). An optical tensiometer (KSV-CAM 100, Finland) was used to measure the contact angles and wettability of electrodes in ambient conditions. An X-ray diffractometer (XRD, Rigaku model, with Cu Kα ($\lambda = 1.54059$)) was used for phase structure characterizations of the electrodes (Ergan and Gengec, 2020). Furthermore, the Scherrer equation was used for the average crystallite size of all phases obtained from the XRD (Kashif et al., 2013; Le et al., 2016).

FT-IR spectrophotometers were used to confirm the functional group of products (Orooji et al., 2020c). The spectra of electrodes were recorded from 4000 to 500 cm^{-1} resolution in the mid-infrared region by a Fourier Transform Infrared Spectroscopy (FT-IR, PerkinElmer, Spectrum 100, USA).

A potentiostat with a three-electrode cell (Gamry Interface 1000, England) was used for Linear Sweep Voltammetry (LSV) and Cyclic Voltammetry (CV) at room temperature. A platinum wire as the counter and saturated calomel electrode (SCE) as the reference electrodes were used. LSV was obtained in a 50-mM Na_2SO_4 solution (pH 3.0) between 0.1 and −1.2 V at a scan rate of 50 mV/s. During LSV measurement O_2 and N_2 were supplied with a flow rate of 16L/h to obtain oxygenated and deoxygenated ambitious, respectively. CV tests were performed in a 10-mM $K_3[Fe(CN)_6]$, and 1.0-M KCl solution (pH 3.0) between −0.4 and 0.8 V at different scan rates (Mousset et al., 2016). Elemental analysis of electrode was realized via CHNS elemental analyzer (Vario Micro Cube).

2.4. Experimental set-up and procedure

A potentiostat with a three-electrode (the produced electrode: working electrode, SCE: reference electrode, platinum wire: counter electrode) cell was used to determine the efficiency of H_2O_2 production. The cell was filled with the 100 mL solution containing 50 mM of Na_2SO_4 at 25 °C. O_2 flow with a rate of 16L/h was used to provide a homogeneous and O_2 saturated solution. The 50 mm × 50 mm of the produced electrode and platinum wire were placed with 3 mm of distance, then the Voltage was set and applied. 2 mL of samples were taken at regular intervals, and the concentration of H_2O_2 was determined. The concentration of H_2O_2 was determined by the iodide method at a wavelength of 351 nm (Özcan et al., 2008) by UV–vis spectrophotometer (DR 6000 model, Hance-Lange GmbH, Germany). The current efficiency (CE) for H_2O_2 production was defined as follows (Xia et al., 2015):

$$CE\ (\%) = \frac{zFC_{H_2O_2}V}{M_{H_2O_2}\ I\ t} \times 100 \quad (4)$$

where, z is the number of electrons transferred for ORR ($2e^-$), F is the Faraday constant (96.485 C/mol), C_{H2O2} is the concentration of H_2O_2 (mg/L), V is the solution volume (0.1 L), $M_{H_2O_2}$ is the molar mass of H_2O_2 (34.01 g/mol), I is the applied current (A), and t is electrolysis time (h). The electrical energy consumption (EEC) (kWh/kg) was calculated from Faraday's law.

$$EEC\ \left(\frac{kWh}{kg}\right) = \frac{1000UIt}{CV} \quad (5)$$

where is the cell voltage (V), *I* is the current (A), *t* is the operating time (h), *C* is the H_2O_2 concentration (mg/L), and *V* is the solution volume (L).

Atrazine removal experiments were also performed in the same cell. The cell was filled with the 20 mg/L of 100 mL atrazine solution at 25 °C and the O_2 with a flow rate of 16L/h. The 50 mm × 50 mm of working electrode and platinum wired were placed with 3 mm of distances. 2 mL of samples were taken at regular intervals, and Atrazine was analyzed by high-pressure liquid chromatography (HPLC, Agilent) equipped with a C18 column (150 mm × 4.6 mm, 5 μm). The mobile phase was selected as a mixture of acetonitrile and water (50:50, v/v) with a flow speed of 0.8 mL/min. Atrazine's intermediates were determined using liquid chromatography quadrupole time-of-flight mass spectrometry (QTOF-LC/MS, Agilent 6200 Series TOF/6500 series Q-TOF). Isocratic elution was 1% formic acid as mobile phase A and acetonitrile with 1% formic acid as mobile phase B with 30/70 (V/V) ratios. 0.3 mL/min of the flow rate and 5 μL of the injection volume were selected. The intermediates of Atrazine were determined by running the instrument in the positive ion scanning mode with a range of 100–2000 *m/z*.

3. Results and discussion

3.1. Characterization of carbon black electrodes

FT-IR spectrum results of the raw and used electrode are depicted in Fig. 1a. The peak intensities are 3430, 2900-2850, 2350, 1630, 1400, 1200,1150, 1050, 800, and 600 cm^{-1} for the raw electrode and 3430, 2900-2850, 2350, 1630, 1380, 1100, 800, 600, and 585 cm^{-1} for the used electrode. The band around 3440 cm^{-1} is due to OH stretching vibration caused by water or hydroxyl groups in the material. This peak intensity shows that the hydroxyl groups for the raw carbon black electrode are reduced after usage. The band at ~2900-2850 cm^{-1} is ascribed to the –CH stretching vibration. The band at around 2350 cm^{-1} is associated with CF_2 backbone for PTFE (Bhullar et al., 2014). The peak at 1630 cm^{-1} and 1400 cm^{-1} are ascribed to the C═C stretching vibration and –COO– stretching vibration, respectively (Yan et al., 2018). The peaks at 1200-1050, 800, and 600 cm^{-1} correspond to $–CF_2$- stretching (Bhullar et al., 2014). The peaks between 1050 and 1200 cm^{-1} and the peak intensities at 800 and 600 cm^{-1} decreased considerably in the used electrode. These peaks belong to $–CF_2$- groups originating from PTFE. In addition, a new peak appeared in the 585 cm^{-1} band in the used electrode, and this band is associated with Fe–O bonds. The presence of this peak shows that there is iron accumulation on the electrode surface after atrazine removal, which causes deactivation of the electrode due to ferric ion complexation (Wang et al., 2018).

Structural features of the raw and used electrodes were determined according to XRD pattern results (Fig. 1b). CB consists of many tiny graphite-like stacks (Chen et al., 2008). Due to the existence of graphite-like structures, the graphitized part of CB contributes to the crystallinity. The more graphitized parts, the higher the crystallinity of carbon black. The mean crystallite sizes were calculated for the raw and used electrode from the XRD patterns using the Scherrer equation were determined as 4.32 and 3.98 Å, respectively. In addition, % crystallinity

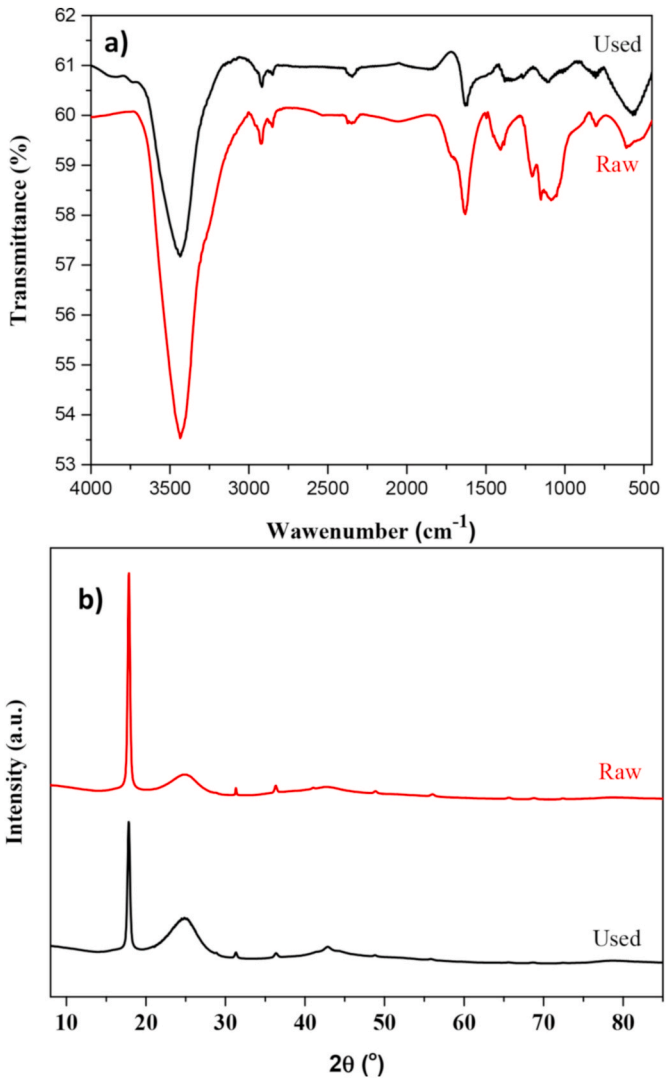

Fig. 1. (a) FT-IR results of the raw and used electrode and (b) XRD results of the raw and used electrode.

values were determined depending on the ratio of the area under the XRD maximum peak to the area under the total peaks. The % crystallinity values of the raw and used electrodes were found as 40% and 67%, respectively. Compared to the raw electrode, the crystallite size of the used electrode decreased, and the % crystallinity value increased in accordance with the literature (Ungár et al., 2005). The mean crystallite sizes at both electrodes are more extensive than graphite (3.354 Å) (Planes and Flandin, 2012) but contain tiny crystals. Small crystallites are not energetically favorable structures. The decrease in the crystallinity of the used electrode after atrazine removal confirms this situation. The XRD peaks of the raw and used electrodes are similar, but the peak intensities at $2\theta = 18$ and $2\theta = 25°$ are different (Fig. 1b). The peak at $2\theta = 18°$ is specific to PTFE, and the intensity of this peak decreased in the used electrode. The large peak (002) at $\theta = 25°$ originates from CB, and the intensity of this peak increased in the XRD pattern of the used electrode. The increase in peak intensity causes by the accumulation of Fe_2O_3, which is observed at the same peak intensity ($\theta = 25°$). This result also overlaps with the FTIR results. Thus it is clear that the presence of Fe accumulation was also supported by the XRD pattern results.

SEM, SEM-EDEX, and contact angle measurements were carried out to examine the change in surface properties of the CB electrode before and after atrazine removal. In Fig. 2, SEM surface images, elemental analysis, and drop profiles obtained from contact angle results are given.

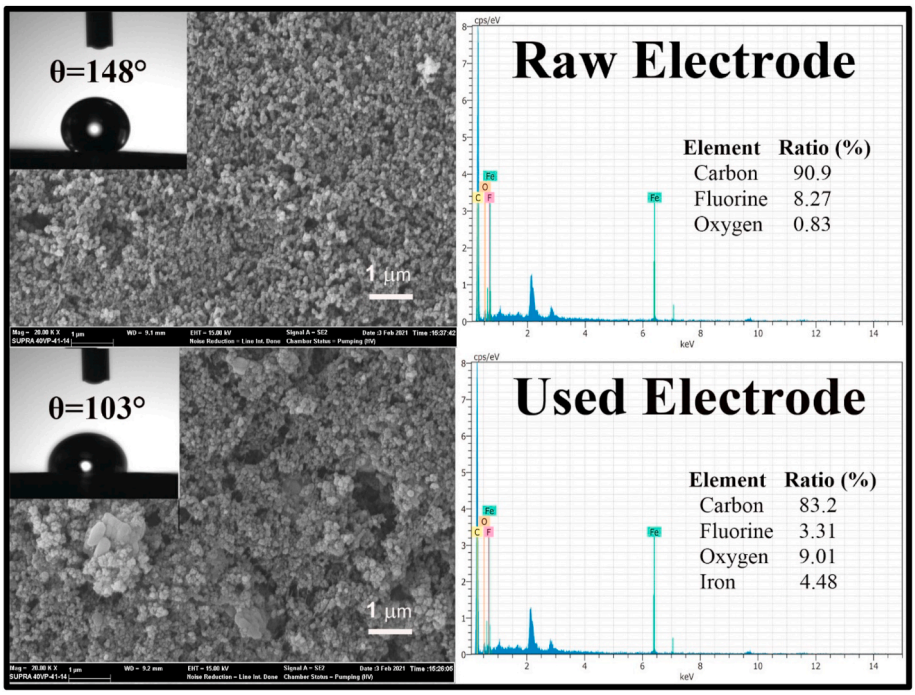

Fig. 2. Contact angle, SEM-EDEX, and SEM images of the raw and used electrodes.

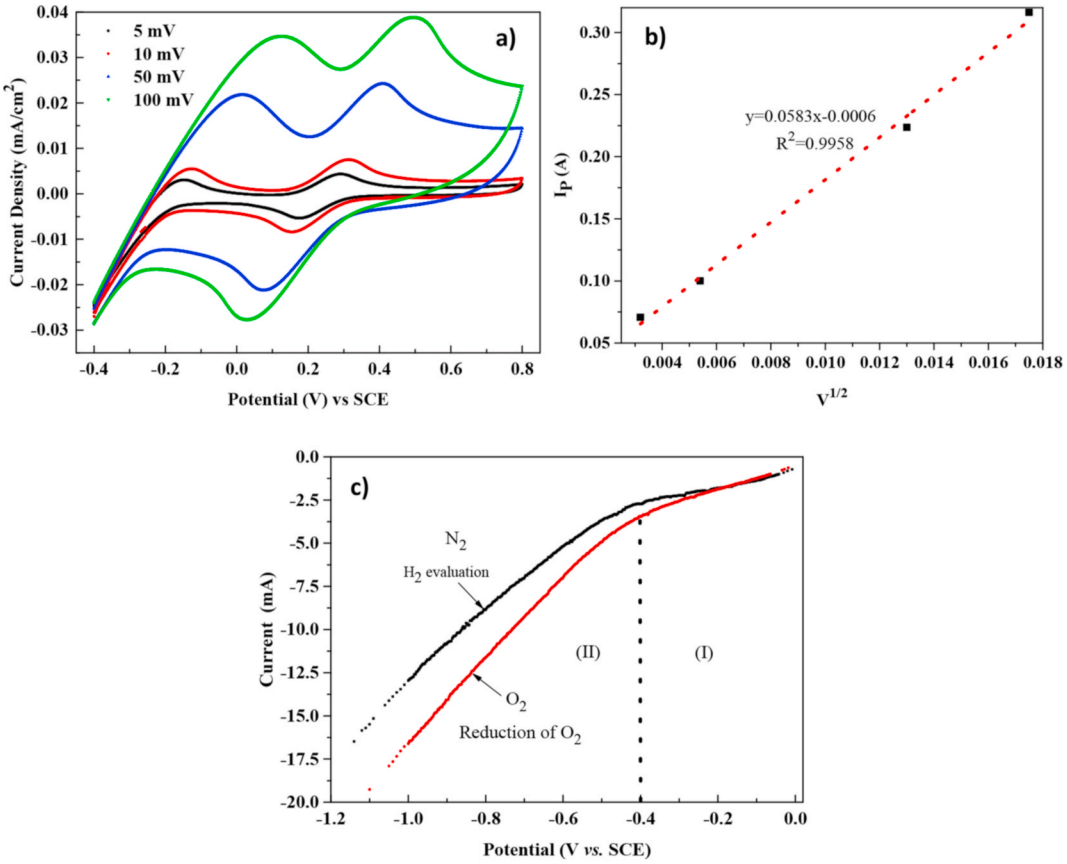

Fig. 3. Electrochemical characterization of the Carbon Black Cathode (a) LSV tests; a 50-mM Na_2SO_4 solution (pH 3.0) at a scan rate of 50 mV/s in an O_2 and N_2 atmosphere with a flow rate of 16L/h. (b) The relationship of the reduction peak current versus the square root of the scan rate $V^{½}$ in the range of 5–50 mV/s and (c) CV tests; 10-mM $K_3[Fe(CN)_6]$, and 1.0-M KCl solution (pH 3.0).

Both surfaces contain roughnesses in the form of micro and nano microfiber (Háková et al., 2018; Orooji et al, 2020a, 2020b). However, as a result of atrazine removal, it is seen that extra roughnesses in the form of micron-sized lumps are formed on the electrode surface, and the spaces between the microfiber-shaped roughnesses on the raw electrode surface are reduced. These results may be due to the change of chemical groups on the surface, as seen in the SEM-EDEX and elemental analysis results. (Fig. 2). The raw electrode surface has carbon (90.9%), fluorine (8.27%), and oxygen (0.83%) composition, while used electrode surface has carbon (83.2%), fluorine (3.31%), oxygen (9.01%), and iron (4.48%) compositions. In other words, after atrazine removal, the fluorine composition has decreased, the oxygen composition has increased, and also iron accumulation has occurred. The smooth Teflon (PTFE) surface has a contact angle of 107° and shows hydrophobic properties (Terzyk et al., 2019). The CB surface shows hydrophilic properties. However, the raw electrode has exhibited superhydrophobic property (148°) due to the porosity of the CB surface and due to the tendency to rise to the surface owing to the low surface energy of the fluorine groups in PTFE. On the other hand, a decrease in the fluorine concentration after atrazine removal caused the contact angle of the electrode used to decrease to 103°, and the electrode exhibited hydrophobic behavior (Gengec et al., 2016). As a result, although raw and used electrodes contain micro and nano roughness, the contact angle value of the used electrode decreased due to decreased fluorine composition after atrazine removal. In addition, the accumulated iron may reduce the contact angle. High hydrophobicity provides high H_2O_2 yield by supporting the mass transfer of oxygen molecules (Jiao et al., 2020; Yang et al., 2018). The raw electrode is more hydrophobic than the used electrode and therefore is expected to have a greater potential to produce H_2O_2.

In this study, Cyclic Voltammetry (CV) measurements were realized to understand the nature of the H_2O_2 production process. Fig. 3a shows the CV curves with different scanning rates (5–100 mV/S) obtained (0.05 mol/L Na_2SO_4 and pH of 3). As shown in Fig. 3a, increasing scan rates causes an increase in the redox peak current while the reduction peak potential shifts to a more negative potential. Furthermore, a linear relationship was observed by the reduction peak current versus the square root of the scan rate $V^{1/2}$ in the range of 5–50 mV/s (Fig. 3b) (Zhu et al., 2020). This phenomenon suggested that the H_2O_2 production process runs under a diffusion-controlled condition.

LSV curves of the electrode in N_2 (deoxygenated) and O_2 saturated solutions can be divided into sections (I) and (II) (Fig. 3c). In section (II), with the negative shift of the potential in solutions saturated with N_2, the current increased significantly. This increase indicates the presence of hydrogen evolution reaction (HER) (Eqn. (6)). Comparatively, the current in the oxygen saturated solution was significantly higher from section (I) than in the deoxygenated solution. Also, this situation is enhanced by the negative potential shift and indicates the electrode's ORR activity (Ghasemi et al., 2020; Raoof et al., 2007; Xia et al., 2015).

$$H^+ + 2e^- \rightarrow H_2 \quad (6)$$

3.2. The effect of experimental conditions on H_2O_2 production

The performance of the electrode for H_2O_2 production was examined in different experimental conditions. First, the effect of initial pH on H_2O_2 production was investigated (Fig. 4a). 253.0, 239.2, 316.2 and 46.1 mg/L of H_2O_2 were obtained after 2 h electrolysis at pH values of 3.0, 5.0, 7.0, and 9.0, respectively. The results obtained in this study showed that the initial pH was highly effective on peroxide production, and the optimal initial pH value was 7, which made the electrode more suitable for in-situ H_2O_2 production because of avoiding the extra addition of acid or alkali. In addition, the highest CE (31.31%) and lowest EEC (10.07 kWh/kg) were both obtained at pH 7.

The second parameter that affects H_2O_2 production yield is the potential. Two main reasons why potential is vital in the EF process are that

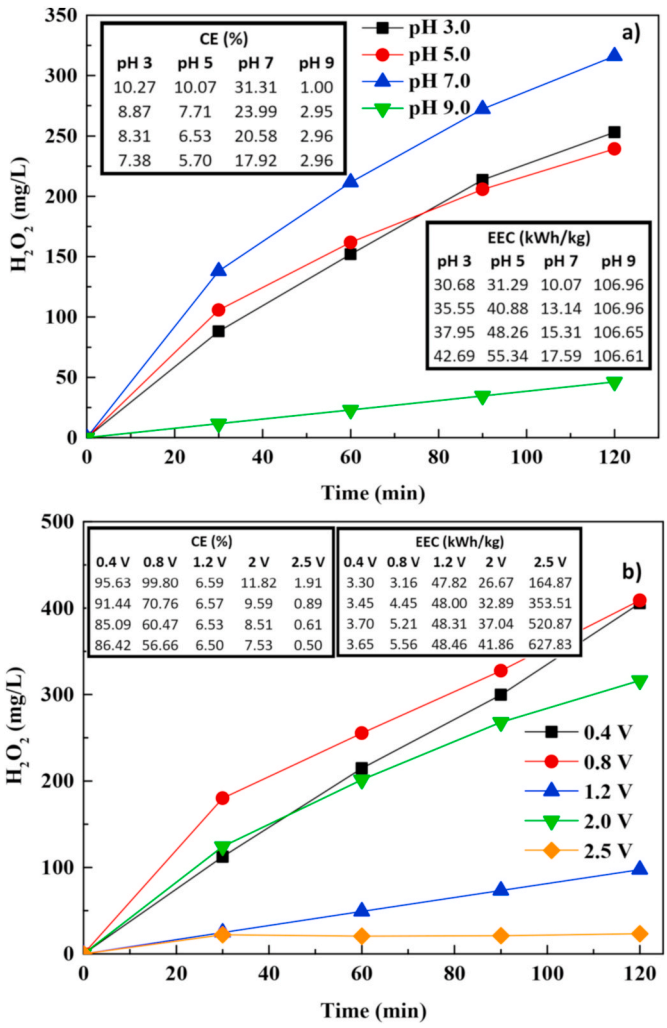

Fig. 4. (a) The effect of pH on the H_2O_2 production capacity of the carbon black electrode at 2 V and (b)The effect of Voltage on the H_2O_2 production capacity of the carbon black electrode at pH 7.0.

it determines the amount of electron transfer required for ORR and the energy consumption of the process. The experiments were realized at 0.4, 0.8, 1.2, 2.0, and 2.5 V. The maximum H_2O_2 production was obtained at 0.8 V as 409 mg/L during 2 h. In addition, the highest CE (99.80%) and lowest EEC (3.16 kWh/kg) values were both obtained at 0.8 V (Fig. 4b).

While examining the effects of both potential and pH on H_2O_2 production yield, the effects of operating time were also examined by taking samples at regular intervals. The increase in operating time positively affects the concentration of H_2O_2 production, unlike EC and EEC. For example, the concentration of H_2O_2 produced at pH 7 increases from 138 to 316 mg/L from the 30th to the 120th minute, while the concentration of CE decreases from 31.31 to 17.92%, and the concentration of EEC increases from 10.07 to 17.59 kWh/kg. Similarly, while the concentration of H_2O_2 increases from 108 to 409 mg/L from the 30th to the 120th minute, the CE decreases from 99.80 to 56.66%, and the EEC increases from 3.16 to 5.56 kWh/kg in the same period. The increased operating time simultaneously promoted the parasitic reactions at the anode (Eqns. (7) and (9)), which cause a decrease in CE.

$$H_2O_2 + 2H^+ + 2e^- \rightarrow 2H_2O \quad (7)$$

$$H_2O_2 \rightarrow HO_2^{\bullet} + H^+ + e^- \quad (8)$$

$$HO_2^{\bullet} \rightarrow O_2(g) + H^+ + e^- \quad (9)$$

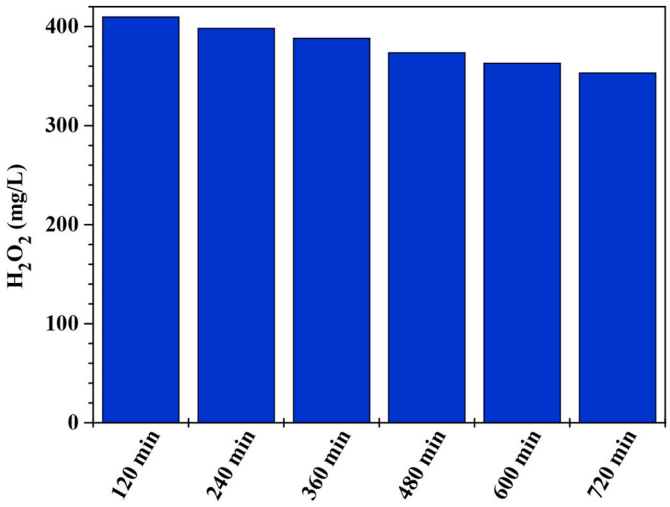

Fig. 5. Stability of Carbon Black cathode for H_2O_2 electrogeneration (pH 7.0 and 2 V).

The concentration of H_2O_2 produced in the EF process is the main parameter that determines the treatment efficiency. However, the stability of the H_2O_2 production, namely the stability of the electrode, becomes more critical in the long term. In experiments (Fig. 5), the electrode had a yield loss of only around 20% during 720 min.

3.3. The effect of experimental conditions on atrazine removal

Unlike the aforementioned part of the study, the effects of experimental conditions (pH, Voltage, catalyst concentration, and operating time) on atrazine removal efficiency are examined separately in this section.

Initial pH can affect the EF process in two different ways. First, as reported above, it can affect H_2O_2 production. Secondly, it affects the species of catalyst (Heidari et al., 2020). The type of iron at different pHs are shown in Fig. 6a (small figure inside) (Kobya et al., 2016) depends on the concentration of iron and the pH of the medium. As well known, the EF process is very effective in the presence of Fe^{+2}, while the presence of Fe^{+3} causes a decrease in treatment efficiency (Li et al., 2020). High pH causes the formation of ferric species, which causes the rapid decomposition of H_2O_2 into oxygen. In this study, the removal efficiencies of 98.7%, 88.6%, 76.4%, and 75.6% were obtained in 5 min at pH of 3.0, 5.0, 7.0 and 9.0, respectively. As seen in Fig. 6a, unlike studies on H_2O_2 production, the fastest removal was obtained at pH 3 due to the nature of the Fenton reaction, which is based on the catalytic reaction being more active at pH 3 ± 0.2 and this result is compatible with the literature (Daneshvar et al., 2008; Nidheesh and Gandhimathi, 2012; Palas et al., 2017; Sandhwar and Prasad, 2017).

As mentioned above, cathode potential has a significant effect on the concentration of H_2O_2 production. Cathode potential has similar but more complex effects on pollutant removal efficiency in the EF process than H_2O_2 production. The change in cathode potential directly affects (i) the concentration of H_2O_2 produced at the cathode, (ii) the concentration of catalyst regeneration, and (iii) the oxidation efficiency at the anode, especially at high potential values (Ergan and Gengec, 2020). As seen in Fig. 6b, atrazine removal efficiency of 18.4%, 75.9%, 59.1% and 98.7% were obtained for 0.4, 0.8, 1.2 and 2.0 V within 5 min. It is concluded that 2 V is the most effective potential, unlike the experimental studies on H_2O_2 production.

In this study, the last parameter examined is the catalyst dosage. With increasing catalyst dosage in the EF process, it is expected that the pollutant removal efficiency will increase to a peak point and then will tend to decrease. The main reason for this expectation is that increased

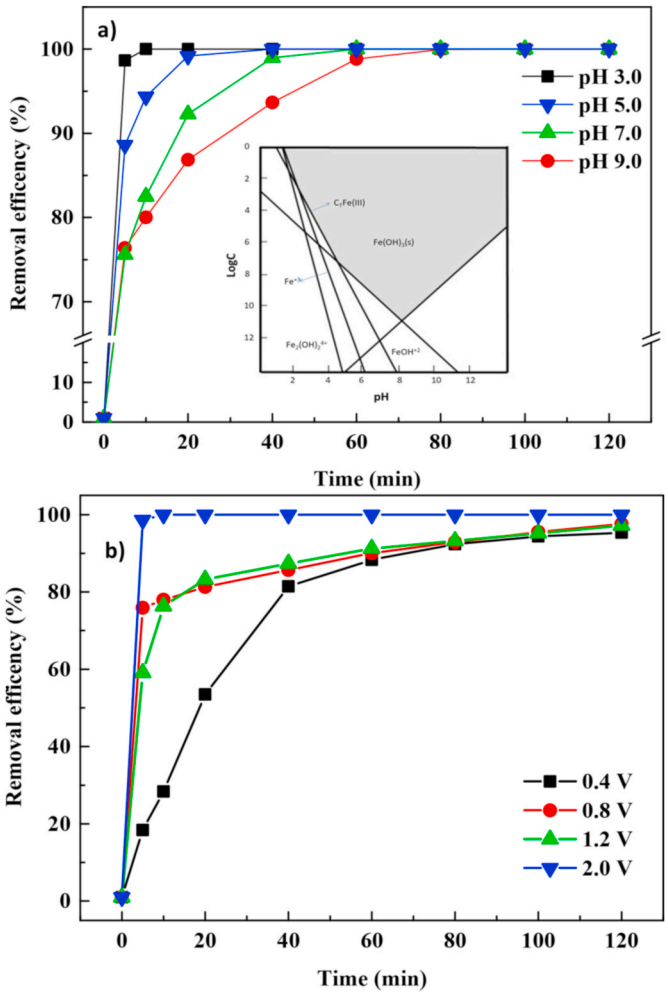

Fig. 6. (a) The effect of pH on the Atrazine removal efficiency (0.3 mM of Fe^{2+} and 2 V) and (b) The effect of Voltage on the Atrazine removal efficiency (0.3 mM of Fe^{2+} and pH 3).

catalyst triggers $OH^{\bullet}$ formation up to a certain point, but overdosing catalyst concentration can cause radical or H_2O_2 depletion by some parasitic reactions (Eqn.(10)–(12)) (Ertugay and Acar, 2017; Palas et al.,

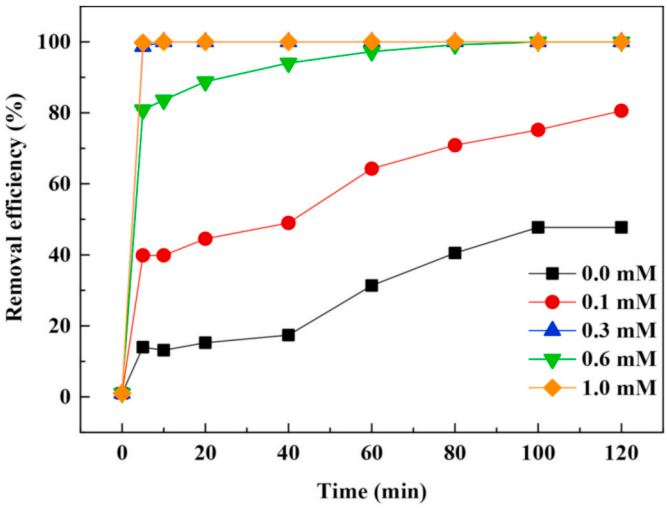

Fig. 7. The effect of Fe^{2+} concentration on the Atrazine removal efficiency (pH 3.0 and 2 V).

2017; Wang et al., 2005). However, it is also possible that overdosing of catalyst causes charge neutralization and coagulation. In this case, the treatment efficiency may not decrease, but the treatment mechanism will turn from oxidation to coagulation. In this study, 0.0, 0.1, 0.3, 0.6, and 1.0 mM of catalyst cause 14.0, 39.9, 98.7, 80.8, and 99.7% of removal efficiencies, respectively (Fig. 7). From these results, it can be concluded that the increase of catalyst increases the removal efficiency up to the optimum dosage (0.3 mM), then removal efficiency decreases due to parasitic reactions (Eqn.(10)–(12)), and finally, the efficiency increases again due to coagulation.

$$Fe^{2+} + OH^{\bullet} \rightarrow Fe^{3+} + OH^{-} \quad (10)$$

$$Fe^{3+} + H_2O_2 \leftrightarrow Fe - OOH^{2+} + H^{+} \quad (11)$$

$$Fe - OOH^{2+} \rightarrow HO_2^{\bullet} + Fe^{2+} \quad (12)$$

3.4. The proposed atrazine degradation pathway in EF process

The degradation by-products of the Atrazine during the EF process were identified by LC-MS with mass to charge (m/z) ratio. The intermediate byproducts determined as hydroxyatrazine (m/z:198) deethylatrazine (m/z: 188), deisopropylatrazine (m/z: 174), deisopropyldeethylatrazine (m/z: 146), allophanate (m/z:104) (Fig. 8). The transformation of Atrazine to by-products occurred via dechlorination, hydroxylation, and dealkylation reactions. The chlorine atom in the Atrazine molecule is rapidly cleaved by the dechlorination reaction and converted to hydroxyatrazine (m/z:198) by the hydroxylation reaction. However, hydroxyatrazine was not found in the mass spectrum because this reaction occurred very rapidly. In addition, Atrazine is converted to deethylatrazine (m/z: 188) and deisopropylatrazine (m/z: 174), by the dealkylation reaction. These two by-products formed in the same way are degraded to deisopropyldeethylatrazine (m/z: 146) with the same dealkylation reaction. Since the hydrogen peroxide production capacity of the electrodes produced during the EF reaction is very high, OH radicals are formed rapidly in parallel with this rapid hydrogen peroxide production. As soon as first 5 min, the degradation products formed with a serious decrease in Atrazine concentration are observed. The chlorine atom in the Atrazine molecule is an easy target to the OH radicals formed during the reaction due to weak C–Cl bonds. Besides chlorine, the aromatic ring of Atrazine can be similarly targeted by OH radicals. Studies have suggested that these type of pesticides derivative has a carcinogenic effect on living tissue due to the chlorine atom in their structure (Mu et al., 2019). It can be concluded that the decomposition products of Atrazine are less toxic due to the cleavage of the chlorine atom in the structure of Atrazine with the reaction and the absence of chlorine atom in the decomposition products formed. If the reaction time is kept long, it is observed that the deisopropyldeethylatrazine (m/z: 146) decomposition product starts to degrade to allophanate (m/z: 104) by breaking the aromatic ring. In addition to removing the chlorine atom from the organic pollutant structure, the deterioration of the aromatic ring structure reveals the efficiency of the process. In conclusion, the conversion of Atrazine to chlorine-free and ring-free decomposition products confirmed the effectiveness of the applied process. However, the process can be modified to complete the mineralization of the aromatic ring structures of the formed chlorine-free degradation products and to carry out the mineralization reaction completely.

4. Conclusions

In this study, carbon fiber as a substrate and a mixture of carbon black and PTFE as the upper layer were used to produce the effective superhydrophobic electrode (148°) for H_2O_2 production and mineralization of Atrazine. Cyclic voltammetry results showed that H_2O_2 production runs under a diffusion-controlled condition. The maximum H_2O_2 production was obtained as 409 mg/L at 0.8 V, 7.0 of pH, and 120 min with the highest current efficiency (99.80%) and the lowest electrical energy consumption (3.16 kWh/kg) values. The electrode stability was evaluated up to 720 min, and after this term, the stability of the electrode reduces about 20%. The reasons for the loss of electrode stability may be the accumulation of the catalyst on the electrode surface and the decrease in PTFE density according to SEM, XRD, and elemental analyzer results. The effects of the operational condition; pH (3.0–9.0), voltage (0.4–2.0 V), operating time (0–120 min), and catalyst concentration (0.0–1.0 mM) in EF were evaluated. The fastest degradation of Atrazine (>99%) is obtained at 2.0 V, 3.0 of pH, and 0.3 mM of Fe^{2+} in 15 min. In the last part of this study, the degradation by-products of the Atrazine during the EF process were monitored by LC-MS. The intermediate byproducts determined as hydroxyatrazine (m/z:198) deethylatrazine (m/z: 188), deisopropylatrazine (m/z: 174), deisopropyldeethylatrazine (m/z: 146), allophanate (m/z:104).

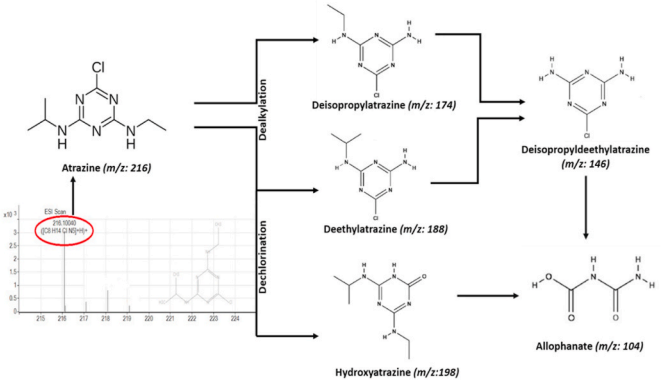

Fig. 8. Proposed degradation of ATZ with EF process.

Credit author statement

Okan Karatas: Conceptualization, Investigation, Data curation.: **Nevin Atalay Gengec:** Conceptualization, Writing – original draft.: **Erhan Gengec:** Conceptualization, Methodology, Validation.: **Alireza Khataee:** Supervision, Writing- Review&Editing.: **Mehmet Kobya:** Supervision, Writing- Review&Editing.

Declaration of competing interest

The authors declare that they have no known competing financial interests or personal relationships that could have appeared to influence the work reported in this paper.

Acknowledgment

We thank the Kocaeli University scientific research project (BAP, Project Number: FMP-2019-1548) for funding the research project.

References

Bhullar, S.K., Bedeloglu, A., Jun, M.B.G., 2014. Characterization and Auxetic Effect of Polytetrafluoroethylene Tubular Structure.

Chen, L., Gong, X.L., Li, W.H., 2008. ARTICLE (in press) POLYMER Effect of carbon black on the mechanical performances of magnetorheological elastomers. https://doi.org/10.1016/j.polymertesting.2007.12.003, 27, 340, 345.

Daneshvar, N., Aber, S., Vatanpour, V., Rasoulifard, M.H., 2008. Electro-Fenton treatment of dye solution containing Orange II: influence of operational parameters. J. Electroanal. Chem. 615, 165–174. https://doi.org/10.1016/j.jelechem.2007.12.005.

Ergan, B.T., Gengec, E., 2020. Dye degradation and kinetics of online Electro-Fenton system with thermally activated carbon fiber cathodes. J. Environ. Chem. Eng. 8, 104217. https://doi.org/10.1016/j.jece.2020.104217.

Ertugay, N., Acar, F.N., 2017. Removal of COD and color from Direct Blue 71 azo dye wastewater by Fenton's oxidation: kinetic study. Arab. J. Chem. 10, S1158–S1163. https://doi.org/10.1016/j.arabjc.2013.02.009.

Gengec, N.A., Cengiz, U., Erbil, H.Y., 2016. Superhydrophobic perfluoropolymer/polystyrene blend films induced by nonsolvent. Appl. Surf. Sci. 383 https://doi.org/10.1016/j.apsusc.2016.04.160.

Ghasemi, M., Khataee, A., Gholami, P., Soltani, R.D.C., Hassani, A., Orooji, Y., 2020. In-situ electro-generation and activation of hydrogen peroxide using a CuFeNLDH-CNTs modified graphite cathode for degradation of cefazolin. J. Environ. Manag. 267, 110629. https://doi.org/10.1016/j.jenvman.2020.110629.

Háková, M., Havlíková, L.C., Chvojka, J., Erben, J., Solich, P., Švec, F., Šatínský, D., 2018. A comparison study of nanofiber, microfiber, and new composite nano/microfiber polymers used as sorbents for on-line solid phase extraction in chromatography system. Anal. Chim. Acta 1023, 44–52. https://doi.org/10.1016/j.aca.2018.04.023.

Heidari, M., Vosoughi, M., Sadeghi, H., Dargahi, A., Mokhtari, S.A., 2020. Degradation of diazinon from aqueous solutions by electro-Fenton process: effect of operating parameters, intermediate identification, degradation pathway, and optimization using response surface methodology (RSM). Separ. Sci. Technol. 56, 2287–2299. https://doi.org/10.1080/01496395.2020.1821060.

Jiang, Z., Li, J., Jiang, D., Gao, Y., Chen, Y., Wang, W., Cao, B., Tao, Y., Wang, L., Zhang, Y., 2020. Removal of atrazine by biochar-supported zero-valent iron catalyzed persulfate oxidation: reactivity, radical production and transformation pathway. Environ. Res. 184, 109260. https://doi.org/10.1016/j.envres.2020.109260.

Jiao, Y., Ma, L., Tian, Y., Zhou, M., 2020. Chemosphere A fl ow-through electro-Fenton process using modi fi ed activated carbon fi ber cathode for orange II removal. Chemosphere 252, 126483. https://doi.org/10.1016/j.chemosphere.2020.126483.

Karimi-Maleh, H., Karimi, F., Fu, L., Sanati, A.L., Alizadeh, M., Karaman, C., Orooji, Y., 2022. Cyanazine herbicide monitoring as a hazardous substance by a DNA nanostructure biosensor. J. Hazard Mater. 423, 127058. https://doi.org/10.1016/j.jhazmat.2021.127058.

Kashif, I., Soliman, A.A., Sakr, E.M., Ratep, A., 2013. XRD and FTIR studies the effect of heat treatment and doping the transition metal oxide on LiNbO3 and LiNb3O8 nano-crystallite phases in lithium borate glass system. Spectrochim. Acta Part A Mol. Biomol. Spectrosc. 113, 15–21. https://doi.org/10.1016/j.saa.2013.04.084.

Khataee, A., Sajjadi, S., Rahim Pouran, S., Hasanzadeh, A., 2017. Efficient electrochemical generation of hydrogen peroxide by means of plasma-treated graphite electrode and activation in electro-Fenton. J. Ind. Eng. Chem. 56, 312–320. https://doi.org/10.1016/j.jiec.2017.07.024.

Khataee, A., Vahid, B., Behjati, B., Safarpour, M., Joo, S.W., 2014. Kinetic modeling of a triarylmethane dye decolorization by photoelectro-Fenton process in a recirculating system: nonlinear regression analysis. Chem. Eng. Res. Des. 92, 362–367. https://doi.org/10.1016/j.cherd.2013.07.019.

Khataee, A.R., Vatanpour, V., Amani Ghadim, A.R., 2009. Decolorization of C.I. Acid Blue 9 solution by UV/Nano-TiO2, Fenton, Fenton-like, electro-Fenton and electrocoagulation processes: a comparative study. J. Hazard Mater. 161, 1225–1233. https://doi.org/10.1016/j.jhazmat.2008.04.075.

Kobya, M., Demirbas, E., Ozyonar, F., Sirtbas, G., Gengec, E., 2016. Treatments of alkaline non-cyanide , alkaline cyanide and acidic zinc electroplating wastewaters by electrocoagulation. Process Saf. Environ. Protect. 105, 373–385. https://doi.org/10.1016/j.psep.2016.11.020.

Le, T.X.H., Charmette, C., Bechelany, M., Cretin, M., 2016. Facile preparation of porous carbon cathode to eliminate paracetamol in aqueous medium using electro-Fenton system. Electrochim. Acta 188, 378–384. https://doi.org/10.1016/j.electacta.2015.12.005.

Li, D., Zheng, T., Liu, Y., Hou, D., He, H., Song, H., Zhang, J., Tian, S., Zhang, W., Wang, L., Ma, J., 2020. A cost-effective Electro-Fenton process with graphite felt electrode aeration for degradation of dimethyl phthalate: enhanced generation of H2O2 and iron recycling that simultaneously regenerates the electrode. Chem. Eng. J. 394, 125033. https://doi.org/10.1016/j.cej.2020.125033.

Mehdizadeh, P., Orooji, Y., Amiri, O., Salavati-Niasari, M., Moayedi, H., 2020. Green synthesis using cherry and orange juice and characterization of TbFeO3 ceramic nanostructures and their application as photocatalysts under UV light for removal of organic dyes in water. J. Clean. Prod. 252, 119765. https://doi.org/10.1016/j.jclepro.2019.119765.

Mousset, E., Wang, Z., Hammaker, J., Lefebvre, O., 2016. Physico-chemical properties of pristine graphene and its performance as electrode material for electro-Fenton treatment of wastewater. Electrochim. Acta 214, 217–230. https://doi.org/10.1016/j.electacta.2016.08.002.

Mu, Y., Zhan, G., Huang, C., Wang, X., Ai, Z., Zou, J., Luo, S., Zhang, L., 2019. Dechlorination-hydroxylation of atrazine to hydroxyatrazine with thiosulfate: a detoxification strategy in seconds. Environ. Sci. Technol. 53, 3208–3216. https://doi.org/10.1021/acs.est.8b06351.

Nidheesh, P.V., Gandhimathi, R., 2012. Trends in electro-Fenton process for water and wastewater treatment: an overview. Desalination 299, 1–15. https://doi.org/10.1016/j.desal.2012.05.011.

Orooji, Y., Ghanbari, M., Amiri, O., Salavati-Niasari, M., 2020a. Facile fabrication of silver iodide/graphitic carbon nitride nanocomposites by notable photo-catalytic performance through sunlight and antimicrobial activity. J. Hazard Mater. 389, 122079. https://doi.org/10.1016/j.jhazmat.2020.122079.

Orooji, Y., Mohassel, R., Amiri, O., Sobhani, A., Salavati-Niasari, M., 2020b. Gd2ZnMnO6/ZnO nanocomposites: green sol-gel auto-combustion synthesis, characterization and photocatalytic degradation of different dye pollutants in water. J. Alloys Compd. 835, 155240. https://doi.org/10.1016/j.jallcom.2020.155240.

Orooji, Y., Mortazavi-Derazkola, S., Ghoreishi, S.M., Amiri, M., Salavati-Niasari, M., 2020c. Mesopourous Fe3O4@SiO2-hydroxyapatite nanocomposite: green sonochemical synthesis using strawberry fruit extract as a capping agent, characterization and their application in sulfasalazine delivery and cytotoxicity. J. Hazard Mater. 400, 123140. https://doi.org/10.1016/j.jhazmat.2020.123140.

Orooji, Y., Tanhaei, B., Ayati, A., Tabrizi, S.H., Alizadeh, M., Bamoharram, F.F., Karimi, F., Salmanpour, S., Rouhi, J., Afshar, S., Sillanpää, M., Darabi, R., Karimi-Maleh, H., 2021. Heterogeneous UV-Switchable Au nanoparticles decorated tungstophosphoric acid/TiO2 for efficient photocatalytic degradation process. Chemosphere 281. https://doi.org/10.1016/j.chemosphere.2021.130795.

Özcan, A., Şahin, Y., Savaş Koparal, A., Oturan, M.A., 2008. Carbon sponge as a new cathode material for the electro-Fenton process: comparison with carbon felt cathode and application to degradation of synthetic dye basic blue 3 in aqueous medium. J. Electroanal. Chem. 616, 71–78. https://doi.org/10.1016/j.jelechem.2008.01.002.

Palas, B., Ersöz, G., Atalay, S., 2017. Çevre dostu atiksu aritimi yöntemleri ile mikrokirletici giderimi kinetiğinin incelenmesi: LaFeO3 perovskit tipi katalizör varliğinda metilen mavisinin Fenton benzeri oksidasyonu. J. Fac. Eng. Archit. Gazi Univ. 32, 1181–1191. https://doi.org/10.17341/gazimmfd.369536.

Paz, E.C., Aveiro, L.R., Pinheiro, V.S., Souza, F.M., Lima, V.B., Silva, F.L., Hammer, P., Lanza, M.R.V., Santos, M.C., 2018. Evaluation of H2O2 electrogeneration and decolorization of Orange II azo dye using tungsten oxide nanoparticle-modified carbon. Appl. Catal. B Environ. 232, 436–445. https://doi.org/10.1016/j.apcatb.2018.03.082.

Planes, E., Flandin, L., 2012. Polymer Composites Bipolar Plates for PEMFCs Polymer Composites Bipolar Plates for PEMFCs. https://doi.org/10.1016/j.egypro.2012.03.031.

Raoof, J.B., Ojani, R., Karimi-Maleh, H., 2007. Electrocatalytic determination of sulfite at the surface of a new ferrocene derivative-modified carbon paste electrode. Int. J. Electrochem. Sci. 2, 257–269.

Ribeiro, J.P., Nunes, M.I., 2021. Recent trends and developments in Fenton processes for industrial wastewater treatment – a critical review. Environ. Res. 197 https://doi.org/10.1016/j.envres.2021.110957.

Sandhwar, V.K., Prasad, B., 2017. Comparative study of electrocoagulation and electrochemical Fenton treatment of aqueous solution of benzoic acid (BA): optimization of process and sludge analysis. Kor. J. Chem. Eng. 34, 1062–1072. https://doi.org/10.1007/s11814-016-0343-8.

Shen, Z., Fan, L., Yang, S., Yao, Y., Chen, H., Wang, W., 2021. Fe-based carbonitride as Fenton-like catalyst for the elimination of organic contaminants. Environ. Res. 198, 110486. https://doi.org/10.1016/j.envres.2020.110486.

Terzyk, A.P., Bryk, P., Korczeniewski, E., Kowalczyk, P., Zawadzka, A., Plociennik, P., Wisniewski, M., Wesolowski, R.P., 2019. 2019Terzyk-PTFE-CA.pdf. Langmuir 35, 420–427. https://doi.org/10.1021/acs.langmuir.8b03790.

Ungár, T., Gubicza, J., Tichy, G., Pantea, C., 2005. 2005Ungar-XRD-crystalinite.pdf. Compos. Part A 36, 431–436.

Wang, A., Qu, J., Ru, J., Liu, H., Ge, J., 2005. Mineralization of an azo dye Acid Red 14 by electro-Fenton's reagent using an activated carbon fiber cathode. Dyes Pigments 65, 227–233. https://doi.org/10.1016/j.dyepig.2004.07.019.

Wang, X., Zhu, K., Ma, X., Sun, Z., Hu, X., 2018. Degradation of diuron by heterogeneous electro- Fenton using modi fi ed magnetic activated carbon as the catalyst †. RSC Adv. 8, 19971–19978. https://doi.org/10.1039/C8RA02776E.

Xia, G., Lu, Y., Xu, H., 2015. Electrogeneration of hydrogen peroxide for electro-Fenton via oxygen reduction using polyacrylonitrile-based carbon fiber brush cathode. Electrochim. Acta 158, 390–396. https://doi.org/10.1016/j.electacta.2015.01.102.

Xuan, T., Le, H., Bechelany, M., Lacour, S., Oturan, N., Oturan, M.A., Cretin, M., 2015. High removal efficiency of dye pollutants by electron-Fenton process using a graphene. based cathode 94, 1003–1011.

Yan, Z., Zhao, H., Han, B., Yang, J., Chen, J., 2018. The suppression of space charge accumulation in CB/LDPE nanocomposites and its association with molecule relaxation. E-Polymers 18, 49–56. https://doi.org/10.1515/epoly-2017-0111.

Yang, Z., Gong, X., Wang, B., Yang, D., Fu, T., Liu, Y., 2018. Magnesium – Carbon Nanotube Composites † 35179–35186. https://doi.org/10.1039/c8ra05907a.

Yao, B., Luo, Z., Yang, J., Zhi, D., Zhou, Y., 2021. FeIIFeIII layered double hydroxide modified carbon felt cathode for removal of ciprofloxacin in electro-Fenton process. Environ. Res. 197, 111144. https://doi.org/10.1016/j.envres.2021.111144.

Zhou, L., Zhou, M., Hu, Z., Bi, Z., Serrano, K.G., 2014. Chemically modified graphite felt as an efficient cathode in electro-Fenton for p-nitrophenol degradation. Electrochim. Acta 140, 376–383. https://doi.org/10.1016/j.electacta.2014.04.090.

Zhou, W., Meng, X., Gao, J., Alshawabkeh, A.N., 2019. Hydrogen peroxide generation from O2 electroreduction for environmental remediation: a state-of-the-art review. Chemosphere 225, 588–607. https://doi.org/10.1016/j.chemosphere.2019.03.042.

Zhu, Y., Qiu, S., Deng, F., Ma, F., Li, G., Zheng, Y., 2020. Three-dimensional nickel foam electrode for efficient electro-Fenton in a novel reactor. Environ. Technol. 41, 730–740. https://doi.org/10.1080/09593330.2018.1509890.